Journal of Petroleum Science and Engineering 162 (2018) 251–259

Contents lists available at ScienceDirect

Journal of Petroleum Science and Engineering

journal homepage: www.elsevier.com/locate/petrol

Mudcake growth: Model and implications

Q. Liu *, J.C. Santamarina

Earth Science and Engineering, KAUST, Saudi Arabia

ARTICLE INFO

Keywords:
Mudcake
Drilling mud
Cement displacement
Thixotropy
Differential pressure sticking

ABSTRACT

Oil and gas account for 60% of the world's energy consumption. Drilling muds that are used to advance oil and gas wells must be engineered to avoid wellbore integrity problems associated with mud cake formation, to favor cake erosion during cementing, and to prevent partial differential sticking. We developed a robust mud cake growth model for water-based mud based on wide stress-range constitutive equations within a Lagrangian reference system to avoid non-natural moving boundary solutions. The comprehensive mud cake growth model readily accommodates environmental factors (e.g., temperature, pH, and ionic concentration) and defines the yield stress distribution for displacement-erosion analyses. Results show that the mud cake thickness is more sensitive to time than to filtration pressure, therefore, time controls the non-uniform distribution of mudcake thickness during drilling. Long filtration time, high permeability, high salinity, high in-situ temperature and low viscosity exacerbate fluid loss and give rise to thick filter cakes. The analysis of residual cake thickness during cement displacement must take into account the effective stress dependent mudcake formation and the time-dependent mud thixotropy. Thixotropy dominates the mud yield stress at high void ratios, e.g. $e > 20$. The offsetting force that causes differential pressure sticking increases sub-linearly as a power function of the still-time.

1. Introduction

The drilling mud removes cuttings from the wellbore, reduces friction between the drill pipe or casing and the wellbore, cools and cleans the bit, coats the formation with a thin, low-permeability filter cake, maintains wellbore stability, and minimizes formation damage. Liquids filtrate into the formation, and solid particles remain behind and form the filter cake against the well wall.

Early research demonstrated that the cumulative flow-through volume is proportional to the square root of time when drilling mud is pressed against a filter paper under conditions of constant pressure and temperature (Larsen, 1938). The filter cake evolves over time but remains inherently inhomogeneous due to the large effective stress gradient that develops across the cake and the ensuing large gradient in porosity and permeability.

The study of mudcake formation and implications has involved experimental as well as analytical and numerical methods. Experimental studies use various techniques that include: dissection (Meeten, 1993; Sherwood and Meeten, 1997), X-ray tomography (Elkatatny et al., 2012) and scanning electron microscopy (Hartmann et al., 1988). Cake formation models typically start with solid and liquid mass conservation equations and incorporate constitutive equations that relate void ratio, effective stress and permeability (Wakeman, 1981; Sherwood et al., 1991; Stamatakis and Tien, 1991; Chenevert and Dewan, 2001; Johansson and Theliander, 2007). Constitutive equations adopted in previous analyses distinguish the “cake phase” from the “slurry phase” and result in “moving boundary” type solutions (Outmans, 1963; Collins, 1976; Stamatakis and Tien, 1991).

This study advanced a comprehensive mudcake growth model for water-based mud based on robust constitutive equations, and used this model to evaluate the influences of time, pressure and environmental factors such as temperature and salinity on the filtration behavior of drilling muds. Subsequent analyses explored critical drilling and completion issues that include mud shearing and differential pressure sticking.

2. Model development

Consider a mud-filled cylinder and a piston that pushes the mud in the cylinder against a pervious formation (Fig. 1a). While liquids filtrate into the formation, solid particles remain behind against the interface. Let's adopt a Lagrangian reference systems fixed in the solid to describe the physical process (see also Sherwood et al., 1991; Sherwood and Meeten, 1997). The boundaries of the Lagrangian element move with the same

* Corresponding author.
E-mail addresses: qi.liu@kaust.edu.sa (Q. Liu), carlos.santamarina@kaust.edu.sa (J.C. Santamarina).

https://doi.org/10.1016/j.petrol.2017.12.044
Received 30 April 2017; Received in revised form 5 December 2017; Accepted 13 December 2017
Available online 15 December 2017
0920-4105/© 2017 Published by Elsevier B.V.

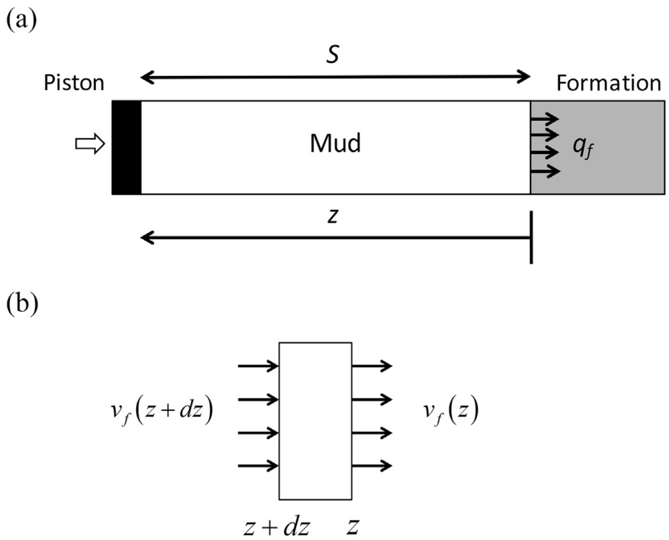

Fig. 1. (a) Schematic representation of the piston model. (b) Infinitesimal element in the Lagrangian system.

velocity as the solid velocity during compression. Fig. 1b shows an infinitesimal element between z and $z + dz$. The fluid mass conservation relates the change in flux through the element to the change in the element void ratio e [Note: void ratio is the volume of voids normalized by the volume of solids and it is related to porosity n as $n = e/(1 + e)$]:

$$[v_f(z+dz) - v_f(z)]dt = -dz[e(t+dt) - e(t)] \tag{1}$$

so that

$$\frac{\partial e}{\partial t} = -\frac{\partial v_f}{\partial z} \tag{2}$$

Darcy's law relates the fluid velocity v_f [m/s] to the permeability of the porous medium k [m^2], the viscosity of the liquid phase μ [Pa·s] and the pressure gradient $\partial u/\partial z$ [Pa/m].

$$v_f = -\frac{k}{\mu(1+e)}\frac{\partial u}{\partial z} \tag{3}$$

Let's substitute Darcy's law into the mass conservation equation to obtain the governing equation for the mud compressed against the pervious wall:

$$\frac{\partial e}{\partial t} = \frac{\partial}{\partial z}\left[\frac{k}{\mu}\frac{1}{1+e}\frac{\partial u}{\partial z}\right] \tag{4}$$

Initially, the mud has a uniform void ratio e_0. The piston imposes a pressure u_0, therefore the filtration pressure is u_0-u_∞, where u_∞ is the constant pressure in the far field inside the formation. As the liquid invades the formation, the effective stress σ' in the mud increases next to the wall in response to changes in fluid pressure u,

$$\frac{\partial \sigma'}{\partial z} = -\frac{\partial u}{\partial z} \tag{5}$$

Therefore, Equation (4) becomes:

$$\frac{\partial e}{\partial t} = -\frac{\partial}{\partial z}\left[\frac{k}{\mu}\frac{1}{1+e}\frac{\partial \sigma'}{\partial z}\right] \tag{6}$$

The mud permeability decreases as the void ratio decreases during cake formation, and the permeability $k = f(e)$ remains inside the derivative. We note that the 1D-formulation developed here presumes a cake thickness much smaller than the well radius. The supplemental material associated with this manuscript includes the non-dimensional form of the partial differential equation (Eq. (6)) and identifies the governing dimensionless ratios.

3. Clay behavior – constitutive equations

The effective stress varies from $\sigma' = 0$ MPa in the slurry, to values that often exceed $\sigma' > 1$ MPa in the mudcake against the formation. Consequently, the void ratios fall from $e > 40$ to $e < 0.5$, and the permeability decreases over 5 orders of magnitude. Surprisingly, these dramatic changes take place within a few millimeters.

Furthermore, in situ conditions are characterized by high temperature and the risk of high salinity contamination. Therefore, we need adequate constitutive models for mud compaction and permeability as a function of effective stress, temperature, and salinity. Table 1 summarizes constitutive equations adopted in previous drilling mud studies. We seek robust, physics-inspired models with a limited number of physically meaningful parameters.

Table 1
Summary of constitutive equations in compressible cake models. Compressibility and Permeability.

Compressibility	Power law	$\frac{(1-n)}{(1-n_0)} = \left(1 + \frac{\sigma'}{\sigma_0}\right)^{\alpha}$	Tiller and Leu 1980, Stamatakis and Tien 1991, Sørensen et al., 1996, Theliander and Fathi-Najafi 1996, Tien and Bai 2003, Johansson and Theliander 2007
		$\frac{n}{n_0} = \left(\frac{\sigma'}{\sigma_0}\right)^{-\alpha}$	Outmans 1963, Holdich 1993, Chenevert and Dewan 2001, Johansson and Theliander 2007
		$\frac{1-n_{avg}}{1-n_{avg0}} = \left(\frac{\sigma}{\sigma_0}\right)^{-\alpha}$	Tiller and Cooper 1962
		$e = e_0 + \left(\frac{\sigma_1}{\sigma' + \sigma_2}\right)^{\alpha}$	Sherwood and Meeten 1997
		$e = e_0 + \left(\frac{\sigma_1}{\sigma'}\right)^{\alpha}$	Carrier and Beckman 1984
	Inverse function	$n = n_0 + \frac{\sigma_1}{\sigma' + \sigma_2}$	Johansson and Theliander 2007
	Logarithm	$e = \alpha \log\left(\frac{-\sigma'}{\sigma_0}\right) + \beta$	Smiles 1970
	Modified semi-logarithmic model	$e = e_c - C_c \log\left(\frac{1kPa}{\sigma' + \sigma'_L} + \frac{1kPa}{\sigma'_H}\right)$	Chong and Santamarina 2016
Permeability	Power law	$k = k_0\left(\frac{\sigma'}{\sigma_0}\right)^{-\beta}$	Tiller and Cooper 1962, Outmans 1963, Holdich 1993, Chenevert and Dewan 2001
		$k = k_0\left(1 + \frac{\sigma'}{\sigma_0}\right)^{-\beta}$	Tiller and Leu 1980, Stamatakis and Tien 1991, Sørensen et al., 1996, Theliander and Fathi-Najafi 1996, Tien and Bai 2003, Johansson and Theliander 2007
		$k = k_0\left(\frac{e}{e_0}\right)^{\beta}$	Ren and Santamarina 2018
	Polynomial	$k = k_0 e^3 (1+e)^{-2}$	Smiles 1970

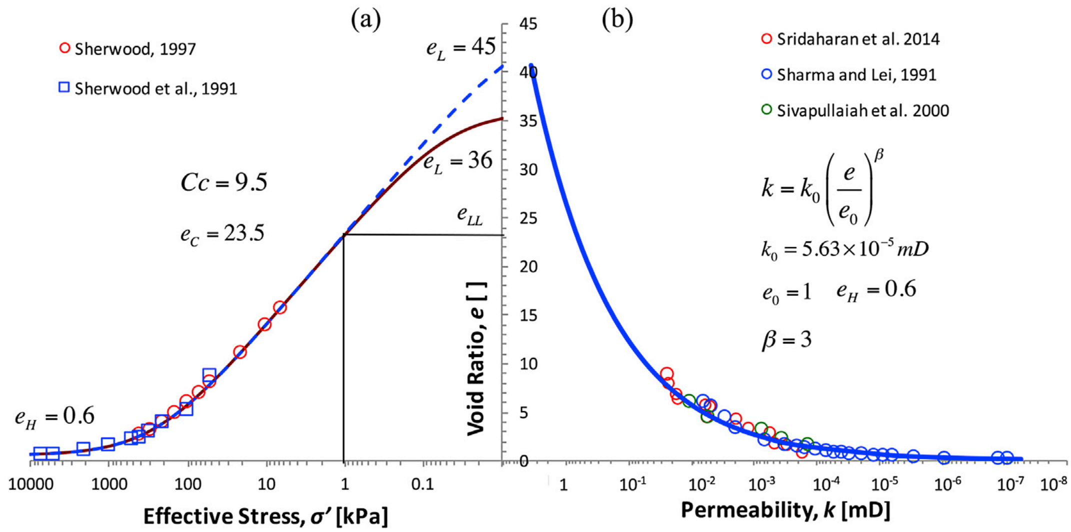

Fig. 2. Constitutive equations of sodium bentonite. (a) Effective stress vs. void ratio. (b) Permeability vs. void ratio (Data from: Sharma and Zongming, 1991; Sherwood et al., 1991; Sherwood and Meeten, 1997; Sivapullaiah et al., 2000).

3.1. Clay structure

Electrical inter-particle forces determine particle aggregation in mineral suspensions. These forces depend on the mineral and fluid chemistry. The drilling industry prefers mono-ionic sodium montmorillonite, where Na^+ cations populate the counter-ion cloud around particles. The fluid pH determines clay edge and surface charges, while the fluid ionic concentration controls the double layer thickness and the balance between attraction and repulsion forces. Consequently, the pore fluid pH and ionic concentration will determine the tendency to disperse or to aggregate into edge–to-face, edge-to-edge, or face-to-face aggregations (Van Olphen, 1977; Santamarina et al., 2001). Other environmental factors such as temperature affect particle association and filtration properties.

The highest void ratio that a packing of platy particles can attain depends on the particle slenderness α, defined as the length L_p divided by the thickness t_p. For example, the void ratio for a card-castle structure can be as high as $e_{max}=(\alpha-1)/2$ (Sharma and Zongming, 1991; Santamarina et al., 2001). The slenderness of montmorillonite particles may reach $\alpha = 100$, which corresponds to a void ratio $e = 50$. This agrees with experimental studies using shear waves (Klein and Santamarina, 2005) and rheological properties (Abend and Lagaly, 2000; Santagata et al., 2008).

3.2. Compressibility

We adopted a wide stress-range compressibility model to avoid the artificially defined cake-slurry interface in the moving boundary problem (Peck and Terzaghi, 1948; Chong and Santamarina, 2016):

$$e = e_c - C_c \log\left(\frac{1kPa}{\sigma' + \sigma'_L} + \frac{1kPa}{\sigma'_H}\right)^{-1} \quad (7)$$

where asymptotic void ratios $e\rightarrow e_L$ and $e\rightarrow e_H$ define the threshold effective stresses σ'_L and σ'_H,

$$\sigma'_H = 10^{(e_C - e_H)/C_C}\,kPa \text{ when } \sigma'\rightarrow\infty \quad (8)$$

$$\sigma'_L = \frac{\sigma'_H}{10^{(e_L - e_H)/C_C} - 1} \text{ when } \sigma'\rightarrow 0 \quad (9)$$

In mud analyses, e_L is the initial void ratio e_0 of the slurry as mixed, $e_L = e_0 \le e_{max}$. Fig. 2 a shows experimental data and model prediction for void ratio versus effective stress e-σ'. In the absence of data at very low effective stress, we note that the void ratio at the liquid limit e_{LL} is a good estimate of the void ratio at $\sigma' = 1$ kPa, $e_{1kPa} \approx e_{LL} = G_S \cdot LL/100$ (Chong and Santamarina, 2016).

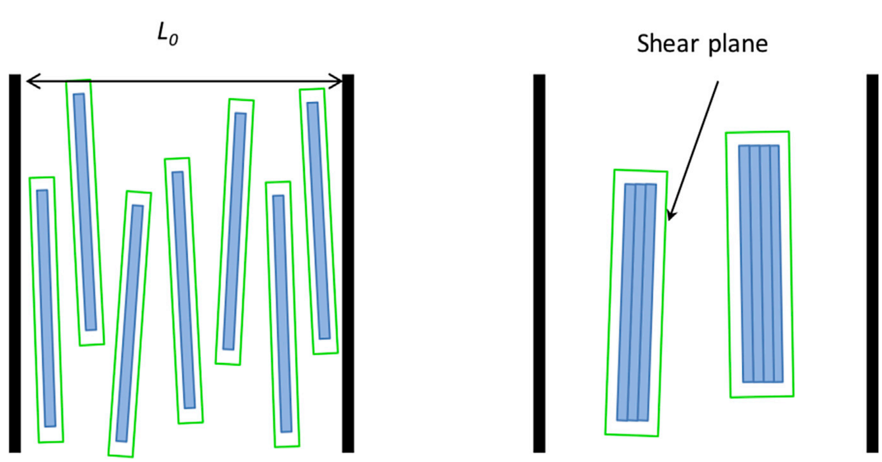

Fig. 3. Impact of environmental factors on the bentonite fabric: dispersed and aggregated clay platelets.

3.3. Fluid flow: permeability vs. void ratio

Permeability decreases as the pore size decreases when the slurry compacts to form the cake. This study adopts a power equation to relate permeability k to the void ratio e (Kozeny, 1927; Carman, 1937; Taylor, 1948; Chapuis and Aubertin, 2003; Ren and Santamarina, 2018):

$$k = k_0\left(\frac{e}{e_0}\right)^{\beta} \tag{10}$$

where k_o is the permeability at the reference void ratio e_0 and the β-exponent captures the sensitivity of permeability to changes in the void ratio. Fig. 2 b shows that this constitutive equation adequately matches experimental data for bentonite. While data are missing at very low effective stress, we highlight that the void ratio at high effective stress dominates the fluid flux across the filter cake.

The proposed constitutive models for compressibility and permeability capture the gradual mud response with effective stress, avoid the non-natural assumptions in moving boundary solutions, and correctly anticipate observed experimental trends (see comparison in supplemental material).

3.4. Temperature: clay rheology and fluid viscosity

Temperature alters the rheological characteristics and the compaction behavior of clay pastes through a combination of competing effects: increased platelet Brownian motion and hindered bond formation, increased Debye-Huckel length and inter-particle repulsion, faster aggregation towards minimum potential energy configurations, and decreased fluid viscosity.

Experimental evidence shows that the yield stress of bentonite suspensions is weakly dependent on temperature below 60 °C and rapidly rises at higher temperature due to the effect of dispersion and increased

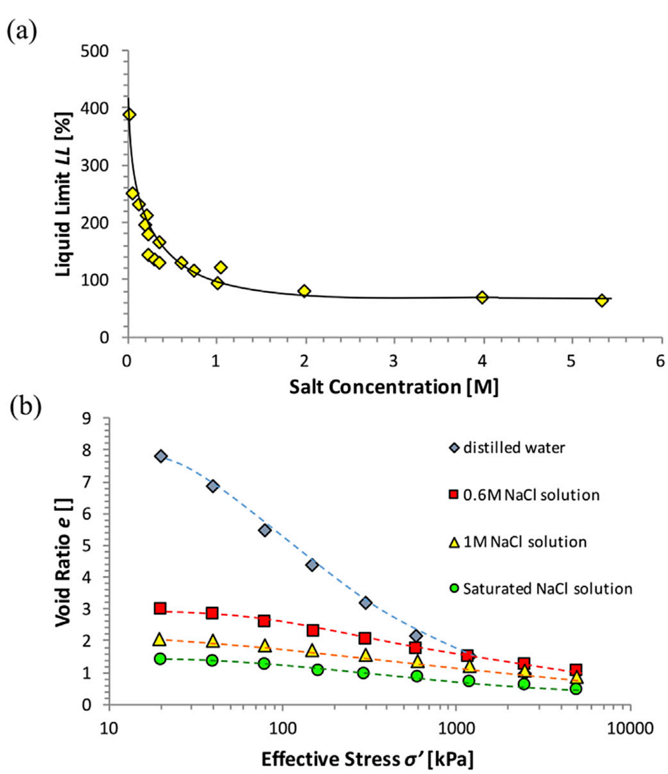

Fig. 4. Environmental factor: ionic concentration. (a) The influence of the salt concentration on the liquid limit of sodium bentonite. Data from: Schmitz and van Paassen, 2002. (b) Odometer curves for bentonite reconstituted with and immersed in NaCl solutions at various concentrations. (Data from: Di Maio et al., 2004).

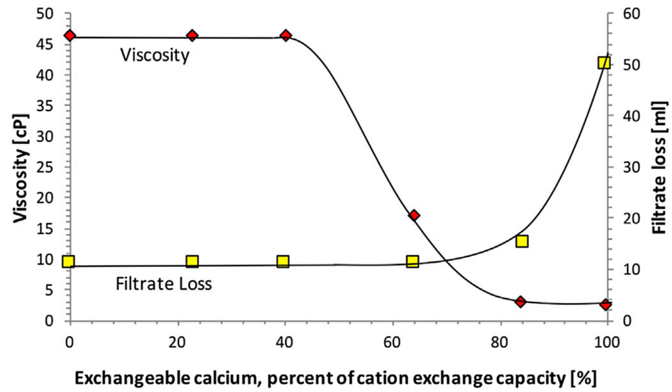

Fig. 5. Viscosity and filtration loss properties at 4% bentonite as a function of the amount of exchangeable calcium. Filtration loss in API tests. (Data from: Williams et al., 1953).

effective mineral surface (Annis, 1967; Alderman et al., 1988). Conversely, a well-dispersed bentonite suspension displays a decrease in the high-shear viscosity as temperature increases (Annis, 1967; Alderman et al., 1988).

Fig. 3 shows the shear plane around dispersed and face-to-face aggregated platelets. Consider n_0 platelets of individual thickness t_p across a representative length scale L_0. When platelets group into n aggregates, the free space L_{free} for fluid shearing depends on the degree of dispersion $\beta = n/n_0$ and the thickness to the shear plane t_{shear}:

$$L_{free} = L_0 - n_0 t_p - 2n t_{shear} = L_0 - n_0\left(t_p + 2\beta t_{shear}\right) \tag{11}$$

Clearly, the fluid free space decreases and the shear resistance $\tau = \mu\nu/L_{free}$ increases with increased dispersion β.

3.5. Fluid chemistry: pH and ionic concentration

Repulsion is shielded, van der Waals attraction prevails and platelets aggregate face-to-face at high ionic concentration, typically above seawater concentration ~0.5 mol/L (see fabric maps in Santamarina et al., 2001; Palomino and Santamarina, 2005). The aggregation of platelets at high ionic concentrations leads to more compacted fabrics, a pronounced decrease in the liquid limit (Fig. 4a) and lower compressibility C_C (Fig. 4b).

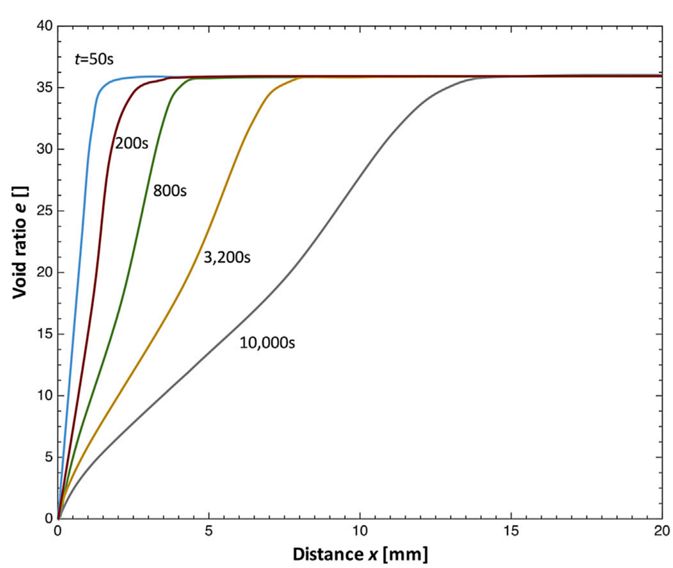

Fig. 6. Cake formation: the influences of filtration time. Void ratio profiles at 50s, 200s, 800s and 3,200s for a 2 MPa filtration pressure. Constitutive parameters are in Table 2.

Table 2
Model parameters.

Permeability $k = k_0 \left(\frac{e}{e_0}\right)^{\beta}$	k_0	5.6×10^{-5} mD
	e_0	1
	b	3
Compressibility $e = e_c - C_c \log\left(\frac{1kPa}{\sigma' + \sigma'_L} + \frac{1kPa}{\sigma'_H} + \right) \sigma'_H = 10^{(e_c - e_H)/C_c} kPa \sigma'_L = \frac{\sigma'_H}{10^{(e_L - e_H)/C_c} - 1}$	e_c	23.5
	e_L	36
	e_H	0.6
	C_c	9.5

Calcium ions replace sodium ions in counter ion clouds, shrink double layers and prompt aggregation. Therefore, mud contamination with calcium ions from gypsum, anhydrite, lime or cement decreases the mud viscosity, increases fluid loss and results in more compact and less compressible cakes (Fig. 5).

4. Cake formation – model predictions

The governing differential equation for cake formation (Eq. (6)), constitutive equations (Eq. (7) and (10)), and mud behavioral trends addressed above (Figs. 2–5) come together in this section, as we explore the mud response during drilling.

4.1. Filtration pressure and filtration time

Let's consider a mud filled borehole. Fig. 6 presents the void ratio profiles under a constant filtration pressure of 2 MPa after 50s, 200s, 800s and 3200s (constitutive parameters listed in Table 2). The cake thickness increases with time. The non-linear *e*-*x* trends reflect the coupling between the non-linear compressibility and permeability models.

Fig. 7 provides void ratio contours along a wellbore after 2.8hr (constant filtration time at all depths). The minimum void ratio attained when the cake rests against the formation ($x = 0$) depends on the filtration pressure. Contour lines for large void ratios $e > 10$ away from the wall are not sensitive to the filtration pressure due to the high compaction next to the formation and the associated low permeability.

4.2. Depth

The filtration time varies with depth during the drilling process. Let's consider a drilling stage from 400 m to 600 m with a rate of penetration $ROP = 20$ m/hr (Fig. 8a). The filtration pressure is 0.8 MPa at 400 m and 1.2 MPa at 600 m with a mud weight = 1200 kg/m^3. Drilling alone takes 10 h so that the filtration time is 10 h at depth 400 m and 0 h at depth 600 m immediately-post drilling (still-time = 0hr). Let's assume a void ratio $e = 10$ as a mud cake thickness criterion. With zero still-time, the corresponding mud cake thickness is 5.8 mm at depth 400 m and 0 mm at depth 600 m. After 24hr of still-time, the filtration time is 34 h at 400 m, 24 h at 600 m, and the corresponding cake thickness has increased to 10.8 mm and 9.1 mm respectively (Fig. 8b). The mud cake thickness becomes more uniform as the still time increases.

4.3. Viscosity of the continuous phase

The viscosity of water decreases with temperature, but it can be augmented by more than two orders of magnitude with the addition of viscosifiers. Let's assume that the change in the viscosity of water does not alter the absolute permeability and compressibility of the bentonite skeleton.

Results in Fig. 9 a&b demonstrate that an increase in the liquid viscosity effectively reduces the fluid loss and leads to a thinner and tighter filter cake. In particular, simulation results show that both fluid loss and cake thickness double when the water viscosity decreases from 1 cP (~20 °C) to 0.3 cP (~90 °C), in good agreement with previous experimental results (Arthur and Peden, 1988). Clearly, filtration properties must be determined at in-situ temperature conditions.

4.4. Permeability

The influence of the permeability on filtration is explored in Fig. 10 for three different values of the reference permeability k_0 that could result from ionic contamination ($k_0 = 1 \times 10^{-5}$ mD, 5×10^{-5} mD and 1×10^{-4} mD. Note: all other constitutive parameters in Table 2 remain the same). Results indicate that more permeable muds form thicker filter cakes and cause more severe fluid loss during filtration. This analysis supports previous experimental results and field observations related to severe fluid losses in the presence of Ca^{2+} or high ionic concentration contamination.

5. Implications

5.1. Cementation: mud replacement and cake removal

Well integrity relies on successful cementing. Inadequate filter cake

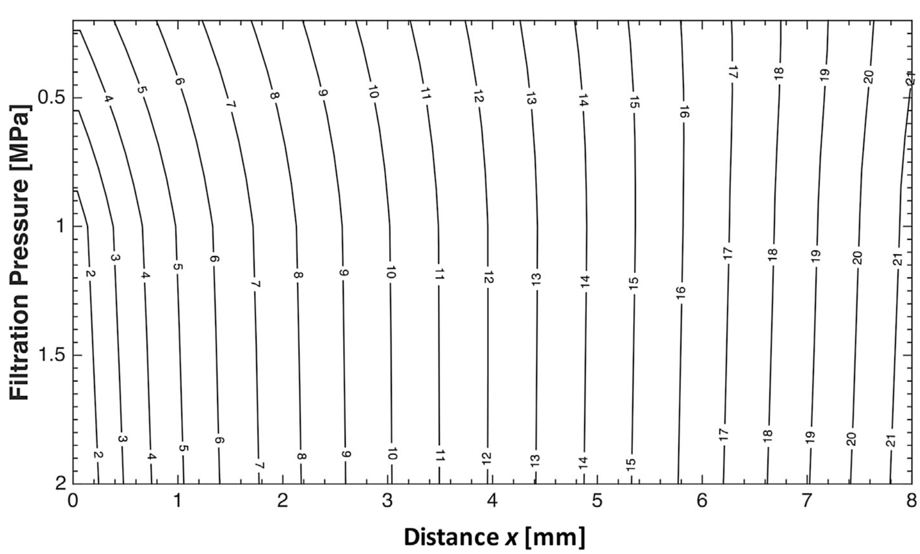

Fig. 7. Cake formation: the effect of filtration pressure. Void ratio contours versus wellbore depth presented in terms of filtration pressure. Filtration time = 2.8 h at all depths.

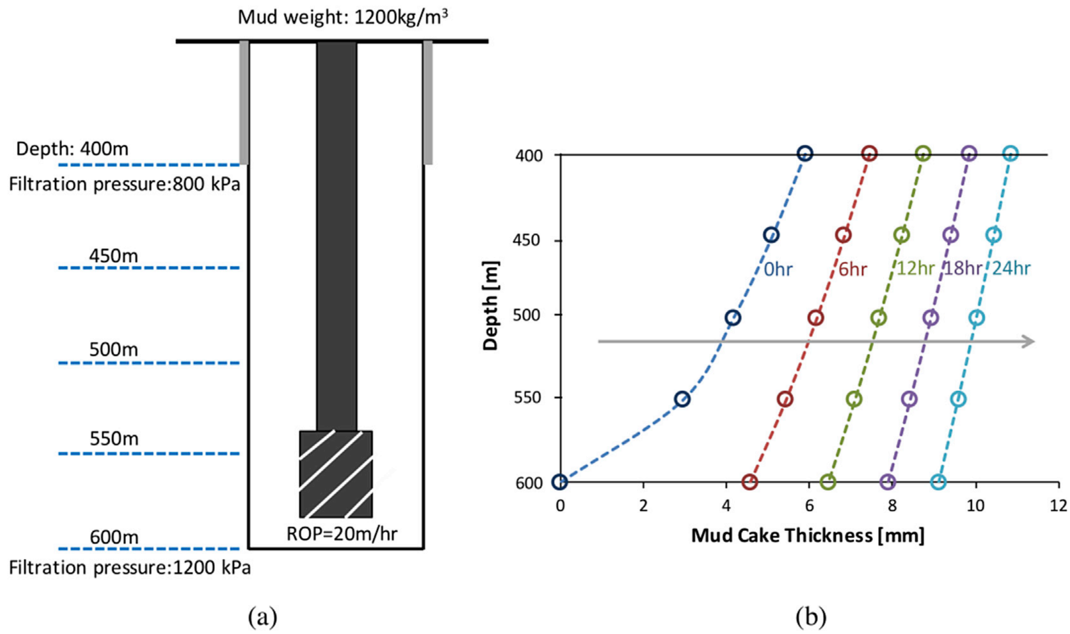

Fig. 8. Cake formation: the effect of time. (a) Case: from 400 m to 600 m depth and rate of penetration ROP = 20 m/hr. (b) Increasing mudcake thickness ($e = 10$) with increasing still-time from 0hr to 24hr.

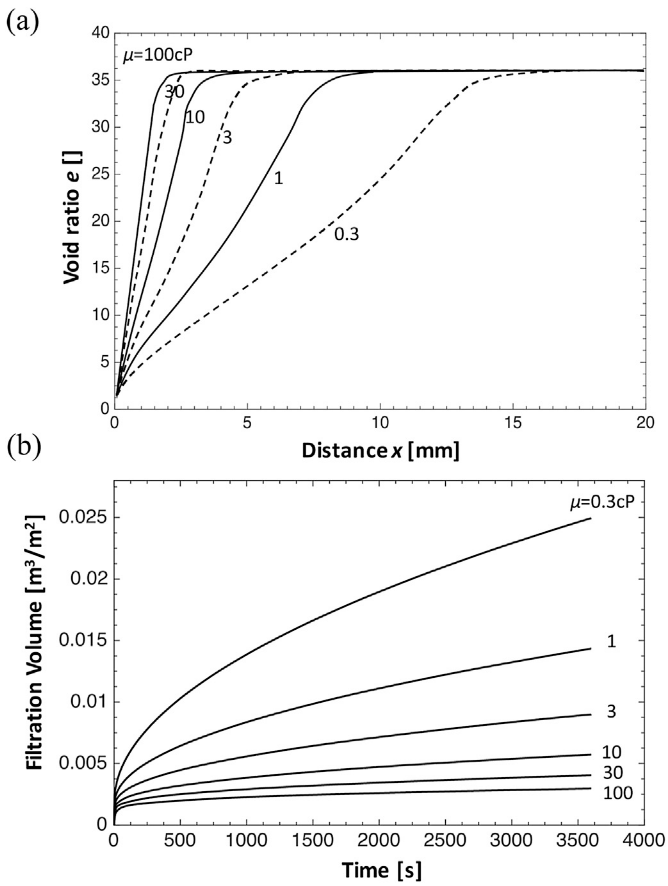

Fig. 9. The influence of the liquid viscosity on the filtration behavior. (a) Void ratio profile. (b) Cumulative filtration volume. Fluid viscosities between 0.3cp and 100cp, filtration pressure = 1 MPa and filtration time = 1hr.

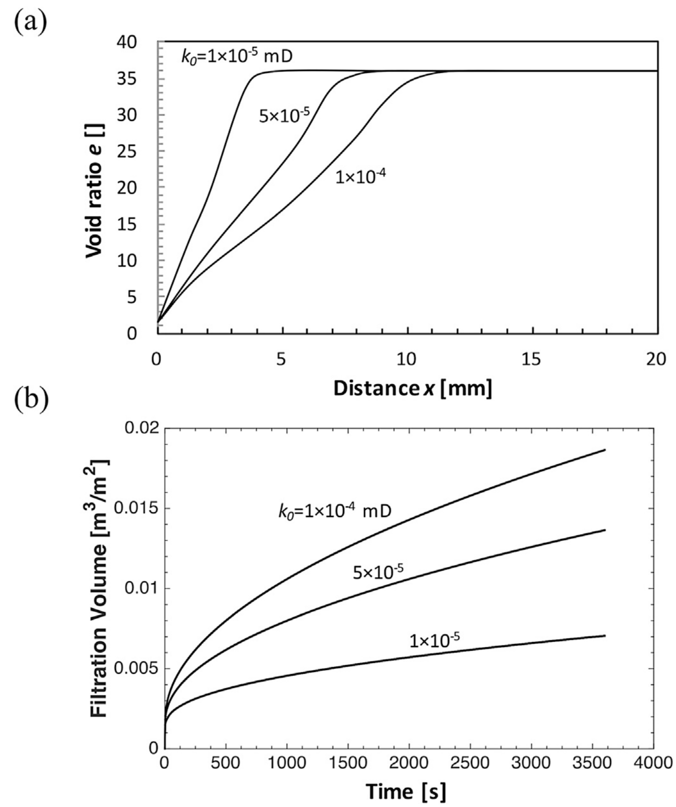

Fig. 10. The influence of permeability on the filtration response. (a) Void ratio distribution. (b) Cumulative filtration volume. Reference permeability $k_0 = 1 \times 10^{-5}$mD, 5×10^{-5}mD and 1×10^{-4}mD, filtration pressure = 1 MPa and filtration time = 1hr.

removal leaves behind a layer of residual cake which may become a potential pathway for gas flow along the annulus (Bonett and Pafitis, 1996). The mudcake is sheared off until the shear stress imposed by the invading cement exceeds the shear strength of the mudcake. The imposed shear stress depends on the displacement velocity in the annulus between the casing and the well wall, and the viscosity of the cement.

On the other hand, the shear strength of the bentonite depends on effective stress in the cake and thixotropic hardening in the slurry. The yield stress of bentonite suspensions is a function of the time t and the

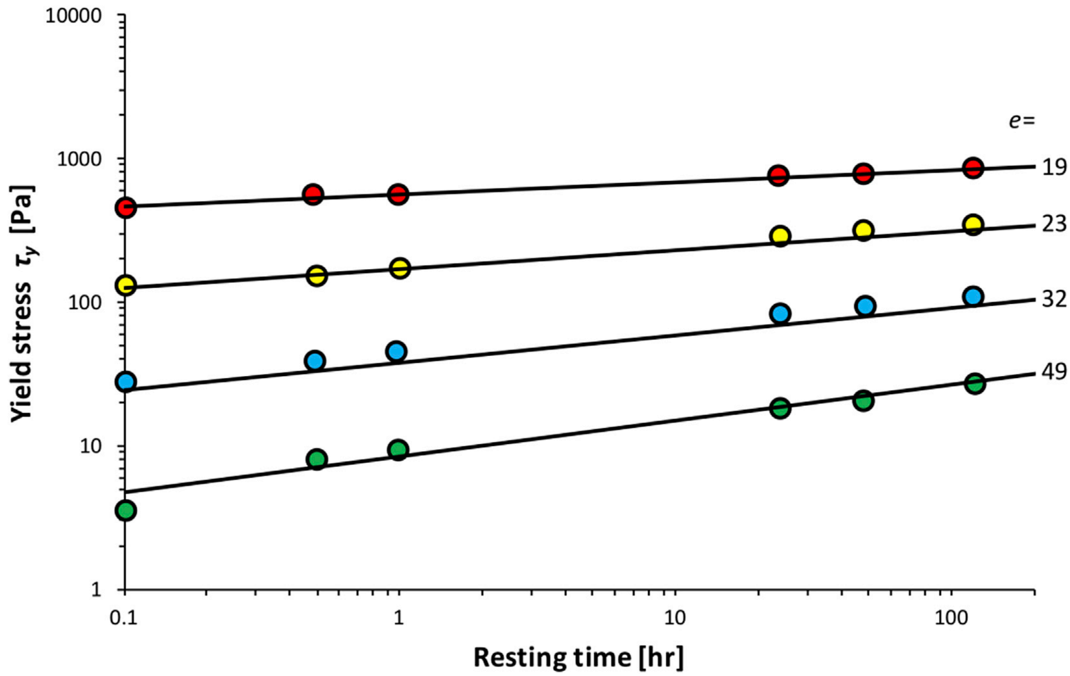

Fig. 11. Thixotropic behavior of bentonite suspension with void ratio $e = 19$, 23, 32 and 49. Solid lines are the model prediction (Equation (12)) and symbols are measured values. (Data from: El Mohtar and Yoon, 2013.

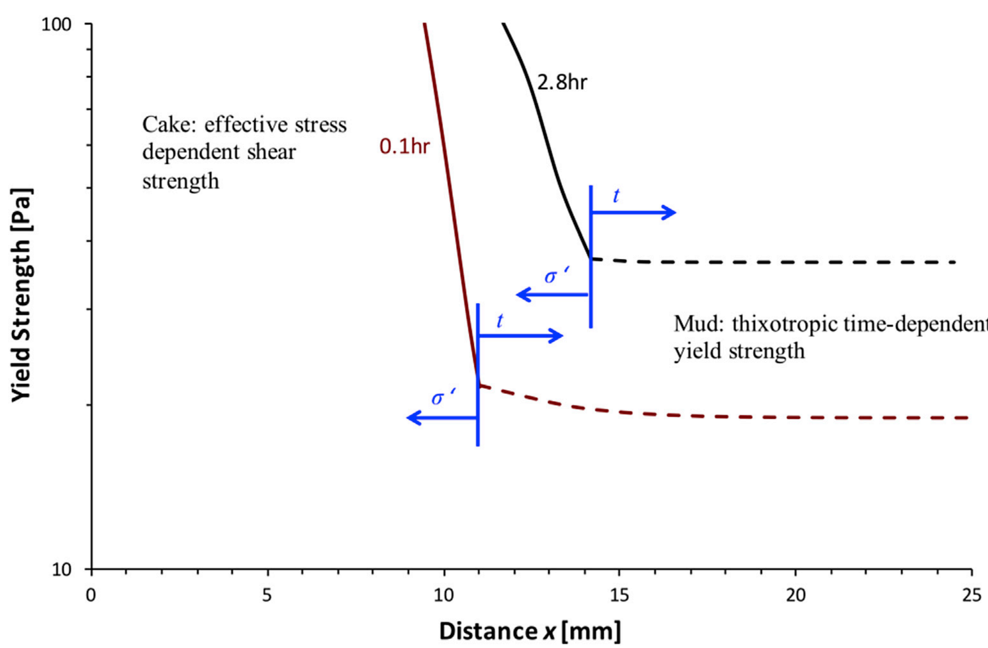

Fig. 12. Yield Strength. Effective stress dependency in the cake, and thixotropic time-dependency in the mud.

void ratio e of bentonite:

$$\tau_y = A\left(\frac{t}{hr}\right)^B \text{Pa} \tag{12}$$

where A is the yield stress τ_y when $t = 1$hr, and B is the sensitivity of τ_y to time. Experimental results in Fig. 11 show that both A and B parameters are a function of the void ratio e:

$$A = 0.42\exp\left(\frac{156}{2.6 + e}\right)$$

$$B = 0.37 - \frac{6.2}{2.6 + e}$$

The effective stress dependent shear strength τ_y in the cake is estimated from the effective stress σ' following a standard Cam Clay formulation (Schofield and Wroth, 1968):

$$\tau_y = 0.2\sigma' \tag{13}$$

We combined these two models to anticipate the shear strength profile of the slurry-mudcake system. Fig. 12 shows the yield stress and shear strength profiles of a filter cake formed under the filtration

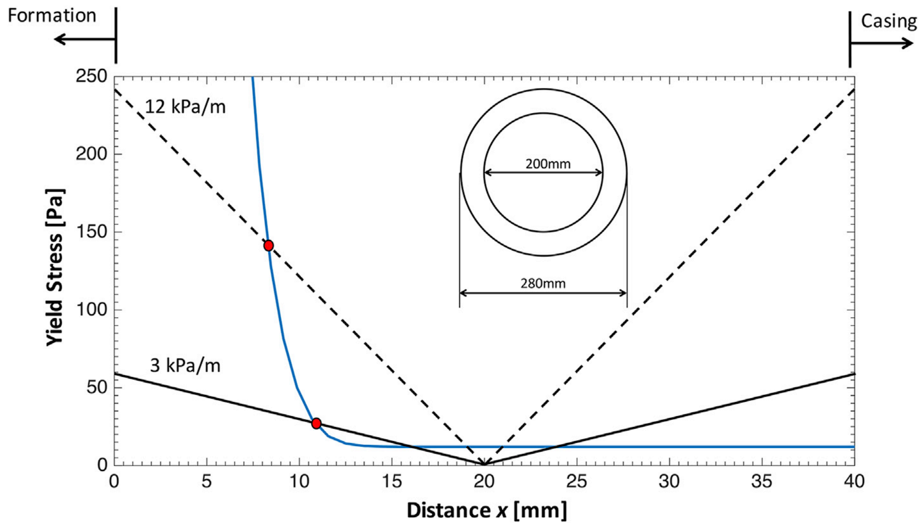

Fig. 13. Residual cake thickness after cement invasion. Black lines: shear stress imposed by the invading cement. Blue line: cake-mud shear strength (refer to Fig. 12). (For interpretation of the references to colour in this figure legend, the reader is referred to the Web version of this article.)

pressure = 2 MPa after 0.1hr and 2.8hr. Results show the combined effect of effective stress and thixotropy: thixotropy dominates the yield stress of muds with high void ratios $e > 20$.

Let's assume a $OD = 200$ mm casing inside a $ID = 280$ mm well so that the annulus is 40 mm thick. The black lines in Fig. 13 are the shear stress profiles imposed by the cement slurry driven by an effective pressure gradient of 3 kPa/m and 12 kPa/m along the well. The intersection point between the yield stress and the shear stress provides a conservative estimate of the residual cake thickness; in this case 11 mm for a pressure gradient of 3 kPa/m and 8 mm for a pressure gradient of 12 kPa/m. The high pressure gradient required to remove the compacted mudcake is not attainable under normal flow conditions. Therefore, the shear stress imposed by the cement slurry is not sufficient for effective mudcake removal.

5.2. *Differential pressure sticking*

"Stuck pipe" events have been one of the drilling industry's major challenges due to lost time and associated costs (Outmans, 1958). In fact, stuck pipes account for about 25% of the non-productive time. A third of the stuck pipes are due to differential pressure sticking (Muqeem et al., 2012).

Mudcake formation has a strong influence on differential sticking incidents. Let's use the cake growth model developed above to determine the force exerted on the tube surface due to unbalanced fluid pressure against the tube. In a polar coordinate system centered with the well (r, θ), the contour of a centered circle is $r = R$ and the contour of an eccentric circle with an offset c satisfies $r^2+c^2\text{-}2r{\cdot}c{\cdot}\cos\theta = R^2$ (Fig. 14.a-inset). The total force T generated by the fluid pressure is the integral of the fluid pressure u against the casing perimeter:

$$T = \int_0^{2\pi} u(r,\beta) R \cos(\beta) d\beta \tag{14}$$

Consider an $ID = 300$ mm borehole filled with mud under a 1 MPa filtration pressure. The $OD = 200$ mm pipe is offset $c = 49$ mm towards a side. Let's assume that the presence of the pipe does not influence the void ratio and pore pressures profiles. Fig. 14.a shows the pore pressure against the well as a function of filtration time. There is a significant fluid pressure drop at $\beta = 180^{\circ}$, where the pipe is closest to the well wall. The total force T acting on the pipe increases sub-linearly with time as the mudcake grows $T = 1.05{\cdot}(t/\text{hr})^{3/4}$ kN/m (Fig. 14 b). This trend resembles earlier experimental studies (Annis and Monaghan, 1962; Reid et al., 1996; Sherwood, 1998). Indeed, minimal time is recommended to reduce stuck pipe complications (Dupriest et al., 2011).

6. Conclusions

This study advanced a comprehensive mudcake growth model for water-based mud implemented with robust, physically-informed constitutive equations. In particular, we adopted wide stress-range constitutive models to avoid numerical discontinuities, and selected compatible

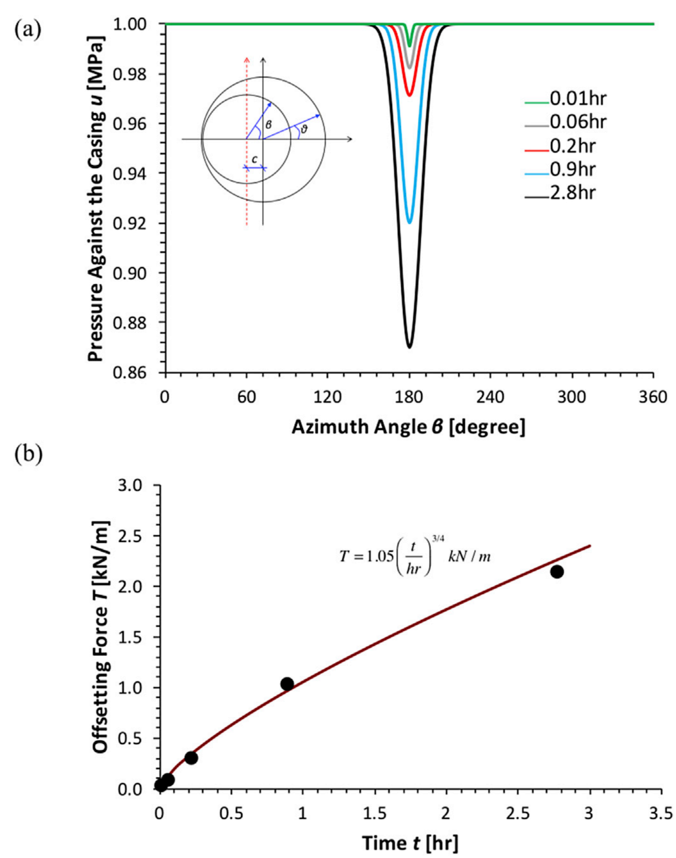

Fig. 14. "Stuck pipe" by differential pressure sticking. (a) Fluid pressure against the casing for a 1 MPa filtration pressure. (b) The effect of the still-time t on the total force against the pipe T.

model parameters for constitutive equations.

The mud cake thickness is more sensitive to time than to filtration pressure. Therefore, time controls the non-uniform distribution of mudcake thickness during drilling. Environmental factors such as temperature, pH, ionic concentration and cation contamination have a significant influence on cake formation. Long filtration time, high permeability, and low viscosity exacerbate fluid loss and increase the cake thickness.

Mud replacement is critical to the quality of the cementing job and the integrity of wellbores. The analysis of residual cake thickness takes into account the effective stress dependent mudcake formation and the time-dependent mud thixotropy. Thixotropy dominates the mud yield stress at high void ratios, e.g. $e > 20$.

Stuck pipe by differential pressure sticking is responsible for costly non-productive time. The offsetting force increases sub-linearly as a power function of the still-time.

Acknowledgements

This research was supported by the KAUST endowment. G. E Abelskamp edited the manuscript.

Appendix A. Supplementary data

Supplementary data related to this article can be found at https://doi.org/10.1016/j.petrol.2017.12.044.

References

Abend, S., Lagaly, G., 2000. Sol–gel transitions of sodium montmorillonite dispersions. Appl. Clay Sci. 16 (3), 201–227.
Alderman, N., Gavignet, A., Guillot, D., Maitland, G., 1988. High-temperature, High-pressure Rheology of Water-based Muds. SPE Annual Technical Conference and Exhibition. Society of Petroleum Engineers.
Annis, M., Monaghan, P., 1962. Differential pressure sticking-laboratory studies of friction between steel and mud filter cake. J. Petrol. Technol. 14 (05), 537–543.
Annis, M.R., 1967. High-temperature flow properties of water-base drilling fluids. J. Petrol. Technol. 19 (08), 1,074–071,080.
Arthur, K., Peden, J., 1988. The Evaluation of Drilling Fluid Filter Cake Properties and Their Influence on Fluid Loss. International Meeting on Petroleum Engineering. Society of Petroleum Engineers.
Bonett, A., Pafitis, D., 1996. Getting to the root of gas migration. Oilfield Rev. 8 (1), 36–49.
Carman, P.C., 1937. Fluid flow through granular beds. Trans. Inst. Chem. Eng. 15, 150–166.
Carrier, W., Beckman, J., 1984. Correlations between index tests and the properties of remoulded clays. Geotechnique 34 (2), 211–228.
Chapuis, R.P., Aubertin, M., 2003. On the use of the Kozeny Carman equation to predict the hydraulic conductivity of soils. Can. Geotech. J. 40 (3), 616–628.
Chenevert, M., Dewan, J., 2001. A model for filtration of water-base mud during drilling: determination of mudcake parameters. Petrophysics 42 (03).
Chong, S.-H., Santamarina, J.C., 2016. Soil compressibility models for a wide stress range. J. Geotech. Geoenviron. Eng. 142 (6), 06016003.
Collins, R.E., 1976. Flow of Fluids through Porous Materials. Petroleum Publishing Co., Tulsa, OK, United States.
Di Maio, C., Santoli, L., Schiavone, P., 2004. Volume change behaviour of clays: the influence of mineral composition, pore fluid composition and stress state. Mech. Mat. 36 (5), 435–451.
Dupriest, F.E., Elks, W.C., Ottesen, S., 2011. Design methodology and operational practices eliminate differential sticking. SPE Drill. Complet. 26 (01), 115–123.
El Mohtar, C., Yoon, J., 2013. Disturbance effect on time-dependent yield stress measurement of bentonite suspensions. Geotech. Test J. 36 (No. 1), 78–87.
Elkatatny, S., Mahmoud, M.A., Nasr-El-Din, H.A., 2012. Characterization of filter cake generated by water-based drilling fluids using CT scan. SPE Drill. Complet. 27 (02), 282–293.
Hartmann, A., Özerler, M., Marx, C., Neumann, H.-J., 1988. Analysis of mudcake structures formed under simulated borehole conditions. SPE Drill. Eng. 3 (04), 395–402.
Holdich, R., 1993. Prediction of solid concentration and height in a compressible filter cake. Int. J. Miner. Process. 39 (3), 157–171.
Johansson, C., Theliander, H., 2007. Validation of predicted local profiles in cake filtration. Chem. Eng. Res. Des. 85 (2), 220–228.
Klein, K., Santamarina, J.C., 2005. Soft sediments: wave-based characterization. Int. J. GeoMech. 5 (2), 147–157.
Kozeny, J., 1927. Über kapillare leitung des wassers im boden:(aufstieg, versickerung und anwendung auf die bewässerung). Hölder-Pichler-Tempsky.
Larsen, D., 1938. Determining the filtration Characteristics of drilling muds. J. Petrol. Eng 42–48.
Meeten, G., 1993. A dissection method for analysing filter cakes. Chem. Eng. Sci. 48 (13), 2391–2398.
Muqeem, M.A., Weekse, A.E., Al-Hajji, A.A., 2012. Stuck Pipe Best Practices-a Challenging Approach to Reducing Stuck Pipe Costs. SPE Saudi Arabia Section Technical Symposium and Exhibition. Society of Petroleum Engineers.
Outmans, H., 1958. Mechanics of differential pressure sticking of drill collars. Petrol. Trans. AIME 213, 265–274.
Outmans, H., 1963. Mechanics of static and dynamic filtration in the borehole. Soc. Petrol. Eng. J. 3 (03), 236–244.
Palomino, A.M., Santamarina, J.C., 2005. Fabric map for kaolinite: effects of pH and ionic concentration on behavior. Clay Clay Miner. 53 (3), 211–223.
Peck, R.B., Terzaghi, K., 1948. Soil Mechanics in Engineering Practice.
Reid, P., Meeten, G., Way, P., Clark, P., Chambers, B., Gilmour, A., 1996. Mechanisms of Differential Sticking and a Simple Well Site Test for Monitoring and Optimizing Drilling Mud Properties. SPE/IADC Drilling Conference. Society of Petroleum Engineers.
Ren, X.W., Santamarina, J.C., 31 January 2018. The hydraulic conductivity of sediments: A pore size perspective. Eng. Geol. 233, 48–54.
Santagata, M., Dalmazzo, D., Santagata, E., 2008. Deformation behavior of clay-water suspensions from rheological tests. In: 4th International Symposium on Deformation Characteristics of Geomaterials (IS-Atlanta). IOS Press, Netherlands, pp. 453–459.
Santamarina, J.C., Klein, A., Fam, M.A., 2001. Soils and waves: particulate materials behavior, characterization and process monitoring. J. Soils Sediments 1 (2), 130–130.
Sharma, M.M., Zongming, L., 1991. A model for clay filter cake properties. Colloid. Surface. 56, 357–381.
Schmitz, R.M., van Paassen, L.A., 2002. The decay of the liquid limit of clays with increasing salt concentration. Newsletter IngeoKring 10 (1), 10–14.
Sherwood, J., 1998. Differential pressure sticking of drill string. AIChE J. 44 (3), 711–721.
Sherwood, J., Meeten, G., 1997. The filtration properties of compressible mud filtercakes. J. Petrol. Sci. Eng. 18 (1), 73–81.
Sherwood, J.D., Meeten, G.H., Farrow, C.A., Alderman, N.J., 1991. Concentration profile within non-uniform mudcakes. J. Chem. Soc. Faraday Trans. 87 (4), 611–618.
Schofield, A., Wroth, P., 1968. Critical State Soil Mechanics.
Sivapullaiah, P., Sridharan, A., Stalin, V., 2000. Hydraulic conductivity of bentonite-sand mixtures. Can. Geotech. J. 37 (2), 406–413.
Smiles, D., 1970. A theory of constant pressure filtration. Chem. Eng. Sci. 25 (6), 985–996.
Sørensen, P.B., Moldrup, P., Hansen, J., 1996. Filtration and expression of compressible cakes. Chem. Eng. Sci. 51 (6), 967–979.
Stamatakis, K., Tien, C., 1991. Cake formation and growth in cake filtration. Chem. Eng. Sci. 46 (8), 1917–1933.
Taylor, D.W., 1948. Fundamentals of Soil Mechanics. LWW.
Theliander, H., Fathi-Najafi, M., 1996. Simulation of the build-up of a filter cake. Filtrat. Separ. 33 (5), 417–421.
Tien, C., Bai, R., 2003. An assessment of the conventional cake filtration theory. Chem. Eng. Sci. 58 (7), 1323–1336.
Tiller, F., Leu, W., 1980. "Basic data fitting in filtration.". J. Chin. Inst. Chem. Eng. 11 (61), 61–70.
Tiller, F.M., Cooper, H., 1962. The role of porosity in filtration: Part V. Porosity variation in filter cakes. AIChE J. 8 (4), 445–449.
Van Olphen, H., 1977. Introduction to Clay Colloid Chemistry. Wiley.
Wakeman, R., 1981. The formation and properties of apparently incompressible filter cakes under vacuum on downward facing surfaces. Trans. Inst. Chem. Eng. 59, 260–270.
Williams, F.J., Neznayko, M., Weintritt, D.J., 1953. The effect of exchangeable bases on the colloidal properties of bentonite. J. Phys. Chem. 57 (1), 6–10.